

# Study of impurity transport in the HL-2A ECRH plasmas with MHD instabilities

Z.Y. Cui<sup>1</sup>, K. Zhang<sup>1</sup>, S. Morita<sup>2</sup>, X.Q. Ji<sup>1</sup>, Y. Xu<sup>1</sup>, X.T. Ding<sup>1</sup>, P. Sun<sup>1</sup>, L.M. Yu<sup>1</sup>, J.M. Gao<sup>1</sup>, W.L. Zhong<sup>1</sup>, C.F. Dong<sup>1</sup>, D.L. Zheng<sup>1</sup>, B.Z. Fu<sup>1</sup>, P. Lu<sup>1</sup>, S.D. Song<sup>1</sup>, M. Huang<sup>1</sup>, Q.W. Yang<sup>1</sup> and X.R. Duan<sup>1</sup>

<sup>1</sup>Southwestern Institute of Physics, P. O. Box 432, Chengdu 610041, China

<sup>2</sup>National Institute for Fusion Science, Toki 509-5292, Japan

*E-mail contact of main author: cuizy@swip.ac.cn*

**Abstract.** An effect of ECRH on the impurity transport has been investigated with relation to the ECRH power deposition in the HL-2A tokamak. A reduction of the impurity concentration is observed in the plasma core when the ECRH power is deposited at the radial locations inside the sawtooth reversal (inner-deposited ECRH). The inverse sawtooth oscillation, i.e. negative ramp and jump, is observed in central channels of soft X ray (SXR) signals, no inverse sawtooth oscillation appears in the ECRH discharges with the power deposition outside the sawtooth reverse (outer-deposited ECRH). Aluminum is injected for the impurity transport study during the ECRH based on the laser blow-off technique. The impurity transport coefficients are analyzed with one-dimensional impurity transport code STRAHL. The analysis shows that the transport of the Al ions is significantly changed between the inner- and outer-deposited ECRH. Both diffusion coefficient  $D$  and convection velocity  $V$  are increased when the ECRH deposition moves inside the sawtooth inversion surface. The outward convection is further enhanced outside the ECRH deposition layer during the inner-deposited ECRH, while the inward convection is generally observed in ohmic discharges. The simulated Al density profile also confirms that the central peaked density profile can be effectively flattened with the inner-deposited ECRH. A long-lasting  $m/n=1/1$  MHD activity combined with an outward heat flux has been observed during the reversed sawtooth case. A change in the impurity transport is discussed with MHD modes.

## 1. Introduction

The role of impurities played in magnetically confined fusion plasmas has been extensively studied so far, since the impurity easily degrades the plasma performance through the radiation loss and the dilution of fuel ions. In the next-generation fusion devices such as ITER, therefore, the reduction of impurity concentration is strictly required for increasing the fusion output. In recent experiments, electron cyclotron resonance heating (ECRH) has been widely used to control the impurity accumulation [1]. Increase in the impurity diffusion at the plasma center and the suppression of pinch effect followed by an inward convection have been observed including reversal to an outward convection [2, 3], when the ECRH is applied. However, the interaction between the edge plasma and the first wall generally becomes strong during the ECRH phase along with the increase of non-thermal electrons. This may cause a serious problem in ITER with high-Z material of tungsten as the plasma facing component. Therefore, a comprehensive understanding on the impurity behaviors during the ECRH phase is important in addition to the impurity transport study. One of possible interpretations for the large increase in the impurity diffusion and the formation of the outward (positive) convection may be done with an enhancement of the turbulence [4]. A flattening of the electron density appeared in the ECRH phase can suggest a reduction of the neoclassical

impurity pinch. Recently, an importance of long-lasting  $m/n=1/1$  MHD activity on the impurity transport at the central ECRH has been reported [5-7] and discussed in the relation between saturated MHD activity and impurity transport.

In this paper, the impurity accumulation in the HL-2A tokamak and its suppression by use of the ECRH are reported. In the ECRH experiment, the effect of sawtooth behaviors on the impurity transport is studied with the laser blow-off (LBO) technique by changing the ECRH power deposition. For the impurity transport analysis one-dimensional (1-D) impurity transport code STRAHL [8] is used. The result is discussed with MHD activities.

## 2. Experimental conditions

The HL-2A is a double-null divertor tokamak with a major radius of  $R = 165$  cm and a minor radius of  $a = 40$  cm. The operation is generally carried out at a toroidal magnetic field of  $B_t = 1.2$ -2.4 T and a plasma current of  $I_p = 150$ -480 kA. The first wall and divertor materials of the present HL-2A tokamak consist of carbon in the main chamber, carbon-fiber composite (CFC) on the baffle and dome, and graphite tiles on the limiter and the armor plate for neutral beam injection (NBI) at inboard vacuum vessel. Then, a fraction of 30% of the vacuum vessel surface is covered with the graphite and CFC materials. A trace impurity for the transport study is injected with a laser blow-off (LBO) system. A YAG laser working at a wavelength of 1064 nm is applied in the energy range of 0.68 –2.0 J. The duration of laser pulse is 10 ns and the diameter of the output beam is 6 mm with a divergence of 0.5 mrad. The metal impurity is coated on a quartz glass substrate by a film thickness of  $\sim 5$   $\mu\text{m}$ . The target installed inside a vacuum tube at mid-plane port of the HL-2A tokamak is located at about 3 meter away from the plasma center. A set of high transmission converging lenses is installed on a step-motor driven translation stage located between the target and laser. The stage can be remotely moved in X and Y directions with a computer in an operation room 50 m away from the experimental room. A multi-shot injection up to 30 Hz is possible in a single plasma discharge using a three-dimensional (3-D) vibration lens for change in the laser beam spot.

As the most dedicated diagnostics to monitor the progression of injected impurity ions radial arrays of soft x-ray (SXR:  $5 \times 20$  channels) and bolometer ( $3 \times 16$  channels) are used in the present study. The temporal and spatial resolutions of the SXR array with a beryllium foil of 25  $\mu\text{m}$  thick are 20  $\mu\text{s}$  and 2.5 cm, respectively, and the response energy ranges in 1–10 keV. The temporal and spatial resolutions of the bolometer system are 50  $\mu\text{s}$  and 2.5 cm, respectively. The total radiation loss can be measured in the energy range of 1 eV–10 keV. The electron density profile in the central column of plasmas ( $r < 25$  cm) is

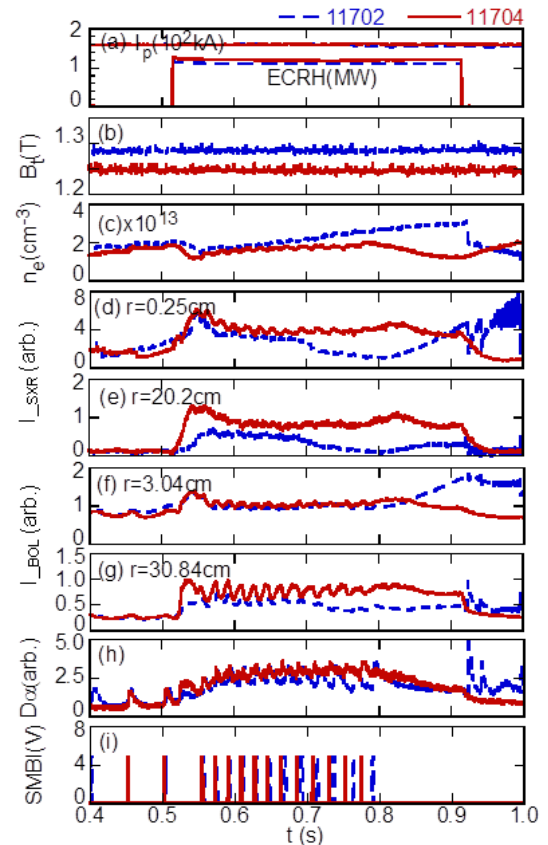


FIG. 1. Time evolution of plasma parameters of two plasma pulses with outer- (#11702) and inner-deposited (#11704) ECRH.

measured with an eight-chord 337  $\mu\text{m}$  HCN laser interferometry and the density profile in the outer plasma region, where the density is less than  $2.0 \times 10^{19} \text{ m}^{-3}$ , is measured with a 26.5 GHz–50 GHz microwave (MW) reflectometer. The electron temperature profile is measured by electron cyclotron emission (ECE) diagnostic calibrated with Thomson scattering diagnostic. The spatial and temporal resolutions of the ECE system are 2 cm and 10  $\mu\text{s}$ , respectively. The ECRH, which is one of the primary heating systems in the HL-2A, consists of six gyrotrons with 68 GHz ( $6 \times 0.5 \text{ MW}$ ) and is generally operated in the second harmonic X-mode when the toroidal magnetic field is low. The power deposition profile of the ECRH can be calculated using a ray-tracing code C3PD. In the present paper, the HL-2A plasma is only heated by the ECRH without using the neutral beam injection (NBI). The ECRH resonance position can be varied between inner- and outer-deposited ECRH by changing the toroidal magnetic field.

### 3. Experimental results

Two discharge waveforms with identical discharge conditions except for toroidal magnetic field are shown in FIG.1. From the top to bottom, plasma current  $I_p$  and ECRH power  $P_{\text{ECRH}}$ , toroidal magnetic field  $B_t$ , line-averaged electron density  $n_e$ , two soft x-ray signals at  $r=0.25$  and 20.2cm and two bolometer signals at  $r=3.04$  and 30.84cm,  $D\alpha$  and timings of supersonic molecular beam injection (SMBI) are plotted. The ECRH deposition layer,  $r_{\text{ECRH}}$ , is then different between the two discharges, i.e. #11702:  $r_{\text{ECRH}} = 10.3 \text{ cm}$  ( $P_{\text{ECRH}}=1.13\text{MW}$ ), #11704:  $r_{\text{ECRH}} = 4.8 \text{ cm}$  ( $P_{\text{ECRH}}=1.12\text{MW}$ ). The line-averaged density for the two discharges is almost the same,  $\sim 2 \times 10^{13} \text{ cm}^{-3}$ , before turning on the ECRH. The sawtooth inversion radii of both discharges are the same as  $r_{\text{inv}} \sim 7.3 \text{ cm}$ , as shown in FIG.2. Therefore, the power deposition layer exists outside and inside the sawtooth inversion for #11702 and #11704, respectively. As shown in FIG.1, the SXR and bolometer signals in #11702 sharply increase at the central channel after switching off the SMBI at 0.79s, while those signals remains unchanged at the edge channel. Such different behaviors in the SXR and bolometer signals between the central and edge channels strongly suggest a different radial profile. Then, a plasma disruption may happen at  $t = 0.92 \text{ s}$  in case of the outer-deposited ECRH in #11702 due to a continuous increase in the impurity radiation. In #11704 with inner-deposited ECRH, on the contrary, all the signals of the electron density, SXR and bolometer do not show any sudden increase during the ECRH phase. The signals also tend to decrease after switching off the SMBI at  $t = 0.79 \text{ s}$ . No plasma disruption occurs in the inner-deposited ECRH discharge. The result indicates that the inner-deposited ECRH

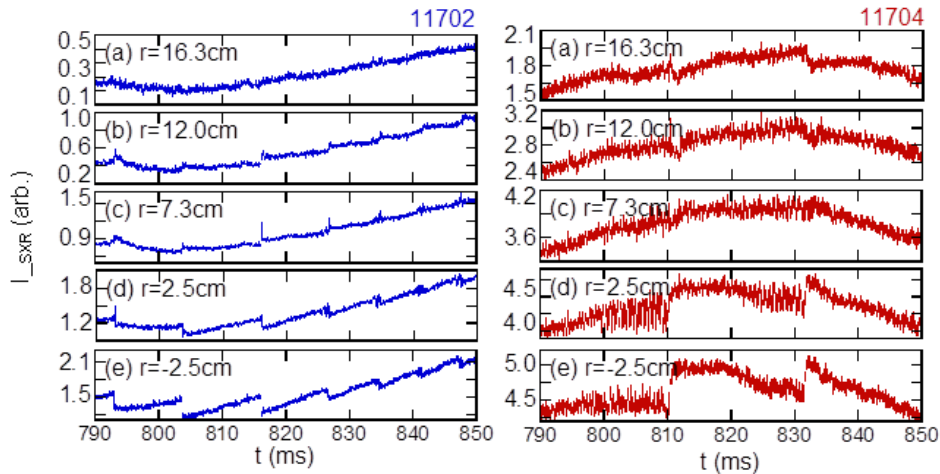


FIG. 2. Time evolutions of SXR at various channels for outer- (left: #11702) and inner-deposited ECRH (right: #11704).

can efficiently make a flatter radiation profile suggesting a mitigation of the impurity accumulation.

Figure 2 shows time evolutions of the SXR signals after switching off the SMBI. A quite different sawtooth behavior is seen in the SXR signals. The time interval of sawtooth oscillation  $\tau_{sw}$  for the outer-deposited ECRH case (#11702) is much shorter ( $\tau_{sw} \sim 10$  ms) than that ( $\tau_{sw} \sim 21$  ms) for the inner-deposited ECRH case (#11704). In addition, the sawtooth ramp and crash are opposite between the two discharges. In the outer-deposited ECRH, the sawtooth behaves a normal oscillation, i.e. positive ramp and crash in the core and negative ramp and jump

outside the inversion radius of  $r_{inv} \sim 7.3$  cm. This sawtooth behavior is generally appeared in the ohmic discharges. In the inner-deposited ECRH, on the other hand, an inverse sawtooth oscillation occurs. It indicates a completely opposite MHD behavior between the two discharges. In addition, a relatively high-frequency mode appears with weak

amplitude at the central channel of SXR signals in the inner-deposited ECRH case (#11704). It is also observed in the electron cyclotron emission (ECE) signals, as discussed later. This inverse sawtooth oscillation and related MHD modes can be only observed in the high-power inner-deposited ECRH discharges of the HL-2A tokamak.

In order to study the effect of the ECRH deposition layer on the impurity transport, aluminum is adopted as an appropriate trace impurity and injected by the LBO system in ECRH discharges with similar plasma conditions mentioned above. The inverse sawtooth oscillation is also confirmed in a set of discharges with inner-deposited ECRH. The temporal behaviors of SXR signals after the Al LBO injection are shown in FIG.3 for two discharges with outer-deposited ECRH (#22710) and inner-deposited ECRH (#22718). The SXR signal quickly increases after the LOB and exponentially decays indicating a certain confinement in the plasma. The signal rise and decay at the central channels in the inner-deposited ECRH (#22718) seems to be faster than that in the outer-deposited ECRH (#22710). The intensity decay time  $\tau_d$  in the central SXR signal can be estimated by fitting with a relation of  $I(t) = I_0 e^{-t/\tau_d}$ . The analysis on the SXR signals gives us a smaller  $\tau_d$  of 50ms for the inner-deposited ECRH (#22718) and a longer  $\tau_d$  of 90ms for the outer-deposited ECRH (#22710). This result indicates that the Al transport is significantly enhanced in the inner-deposited ECRH case. The Al transport is studied with a one-dimensional (1-D) impurity transport code.

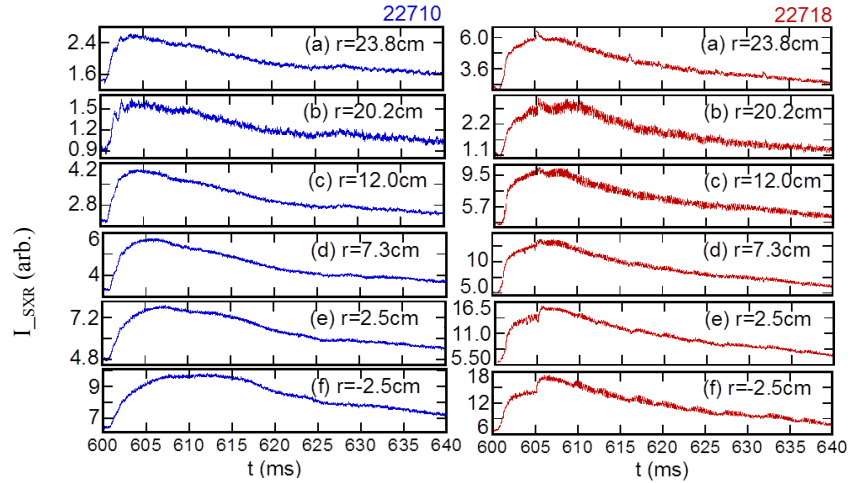


FIG. 3. Time evolutions of SXR signals after Al injection with outer- (#22710) and inner- (#22718) deposited ECRH.

#### 4. Estimation of impurity transport coefficients

A radial impurity transport code [8], STRAHL, has been used in the present study. In this model the radial flux of impurity ions is expressed as the sum of diffusive and convective terms;

$$\Gamma_z(r) = -D(r) \frac{\partial n_z(r)}{\partial r} + V(r)n_z(r) \quad ,$$

(1)

where  $D(r)$  and  $V(r)$  are the diffusion coefficient and the convection velocity, respectively. Both values are assumed to be time independent and averaged over all the ionization stages of impurity. STRAHL solves the system of time-dependent continuity equations for all the ionization stages of impurity by an equation of

$$\frac{\partial n_z}{\partial t} + \nabla \Gamma_z = n_e (S_{z-1}n_{z-1} + \alpha_{z+1}n_{z+1}) - n_e n_z (S_z + \alpha_z) + s_z \quad ,$$

where  $S_z$  and  $\alpha_z$  denote the ionization and recombination rate coefficients of the ionization stage of  $z$ , respectively, and  $s_z$  is the external source term. The coefficients of  $S_z$  and  $\alpha_z$  provided by Atomic Data and Analysis Structure database (ADAS) [9] are used. The measured electron density and temperature profiles are the input plasma parameters for the code in addition to the magnetic field strength and  $q$  factor at the last closed flux surface (LCFS).

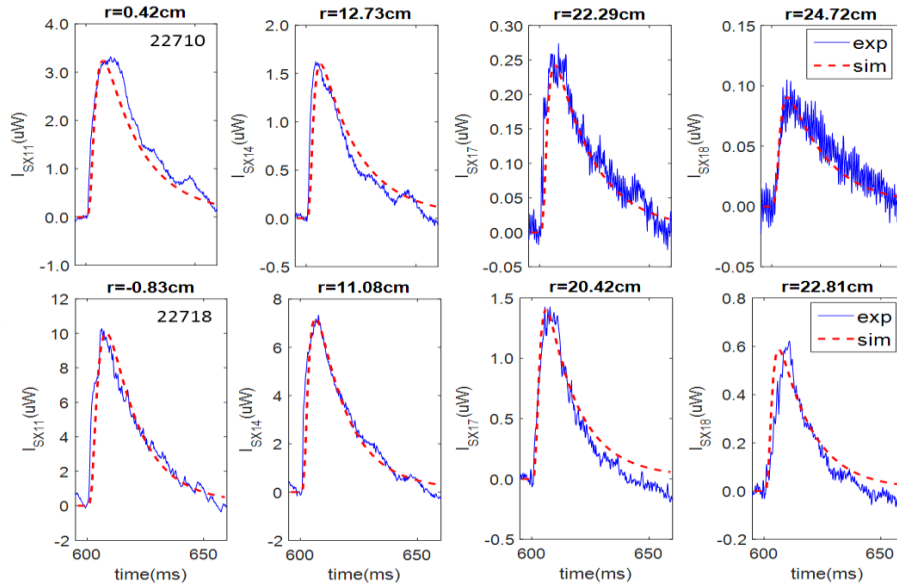


FIG. 4. Comparison of SXR intensity between experiment and simulation for outer- (top: #22710) and inner- (bottom: #22718) deposited ECRH.

The STRAHL code starts the simulation at an initial guess of the transport coefficient profiles. It solves the coupled continuity equations and reconstructs the measured emission, such as the SXR and bolometric signals. Then, the transport coefficients are modified iteratively until the difference between the reconstructed signals and the measured ones is minimized in the least squares ( $\chi^2$ ) sense [10]. In order to reduce the error of the Abel inversion, the line-of-sight integrated SXR brightness is simulated. The comparison between the simulation (dashed lines) and the experiments (solid lines) are shown in FIG.4

for both the outer- (#22710) and inner- (#22718) deposited ECRH discharges. A good fitting is obtained for the SXR temporal behaviors in two discharges.

The analyzed radial profiles of corresponding diffusion coefficient  $D(r)$  and convective velocity  $V(r)$  are plotted in FIG. 5. Here,  $\rho$  is the normalized plasma radius. The result indicates that the  $D$  is large in the outer plasma region,  $D=6 \text{ m}^2/\text{s}$ , while it is much smaller in the plasma center,  $D=1 \text{ m}^2/\text{s}$ . The result on the  $V(r)$  shows more complicated profiles. The  $V$  takes negative values at the plasma central region and positive values in the plasma outer

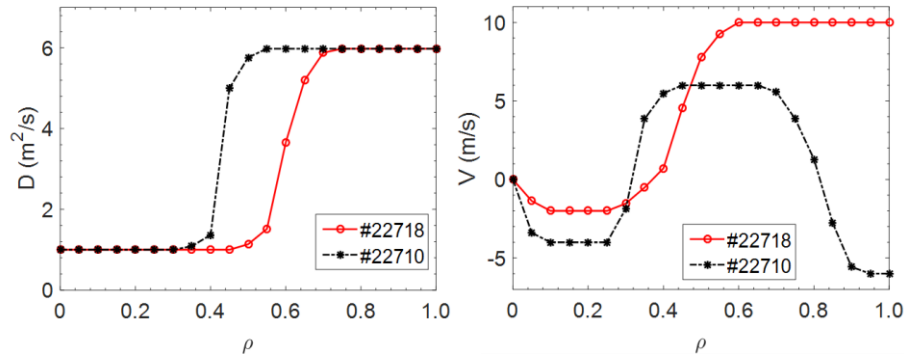


FIG. 5. Simulated transport coefficients of outer- (#22710) and inner- (#22718) deposited ECRH.

region for both discharges, indicating the inward and outward convection, respectively. The  $V$  drops to negative values again in case of the outer-deposited ECRH. This originates in the slower decay time in the SXR signal at the outermost channels (see #22710 in FIG. 4). The obtained impurity diffusion coefficients are much larger than the neoclassical predictions which can be also calculated with the STRAHL code (not presented in FIG. 5). Seeing in FIG. 5, it is clear that the  $V$  for the inner-deposited ECRH (#22718) shows larger outward convection at the outer plasma radii compared with the outer-deposited ERH (#22710). It means the outward flux of Al ions is significantly enhanced by the central deposition of ECRH. This result is also in good agreement with the previous result [11].

The simulated density profile of Al ions is compared between the two discharges in FIG.6. The Al influx from the LOB in #22710 seems to be slightly larger than that in #22718 just after the Al impurity is injected. The Al density profile becomes slightly hollow or flat in the inner-deposited ECRH (#22718), while it becomes peaked at the plasma center in the outer-deposited ECRH (#22710). The present result demonstrates that the impurity accumulation can be effectively weakened when the ECRH deposition layer is located inside the sawtooth reversion surface.

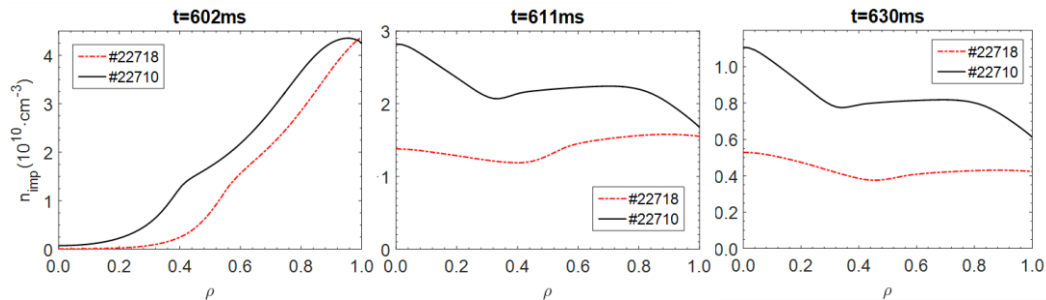


FIG. 6. Comparison of impurity density profiles between outer- (#22710) and inner- (#22718) deposited ECRH.

## 5. Discussions and summary

The effect of ECRH deposition layer on the impurity transport has been investigated in the HL-2A tokamak. When the ECRH power deposits inside the sawtooth inversion layer ( $r_{\text{ECRH}} < r_{\text{inv}}$ ), the impurity accumulation can be reduced. The sawtooth oscillation is inverted when the ECRH power is deposited in the plasma center. The time interval of the sawtooth oscillation becomes considerably long ( $\tau_{\text{ST}} \sim 20$  ms) in the inner-deposited ECRH case, while it is much shorter in the outer-deposited ECRH case and also in the ohmic discharges ( $\tau_{\text{ST}} \sim 10$  ms). The inverse sawtooth oscillation can be only observed in the high power inner-deposited ECRH discharges ( $P_{\text{ECRH}} > \sim 1$  MW) in the HL-2A tokamak.

In addition, a  $(m, n) = (1, 1)$  MHD activity existed for typically  $0.5 \times \tau_{\text{ST}}$  before the next sawtooth crash is observed at the central channels of SXR with the inner-deposited ECRH case. When this mode appears, an outward heat flux is also observed with the ECE measurement. The result is shown in FIG.7 for a discharge with inner-deposited ECRH ( $P_{\text{ECRH}}=1.2\text{MW}$ ). A steep rise just after the crash measured with SXR signal is plotted in FIG.7 (a) for showing a typical behavior of the inner-deposited ECRH. The ECE signals from central to edge channels are shown in FIGS. 7(b)-(g). It clearly shows that the heat flux propagates from the plasma core to the edge during the period of the mode. Considering the outward flow of the heat flux, it may suggest an enhancement of the impurity transport.

The MHD activities are analyzed with relation to the ECRH deposition layer. The time trace of the SXR signals and the frequency spectrum are shown in FIGS. 8(a) and (b) for the outer- and inner-deposited ECRH, respectively. A low-frequency MHD mode is newly appeared around  $f_{\text{MHD}} \sim 2\text{-}3\text{kHz}$  which is coincided with the sawtooth oscillation. This may be also

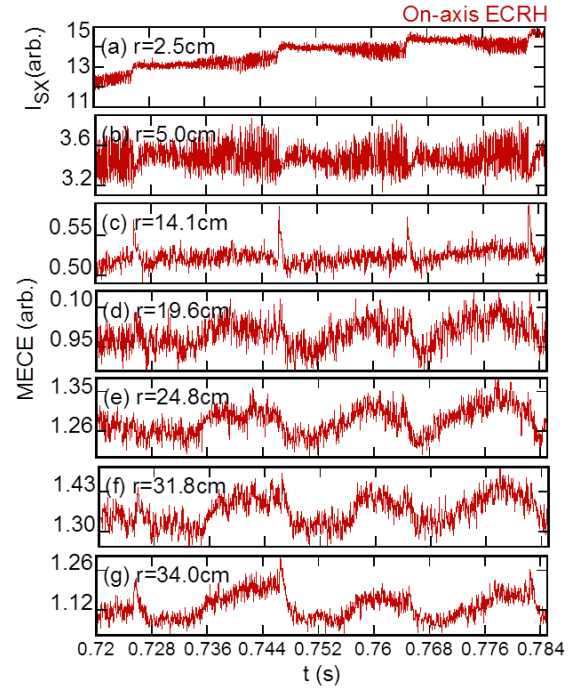


FIG. 7. Time evolutions of (a) central SXR and (b)-(g) ECE signals at various channels for inner-deposited ECRH discharge.

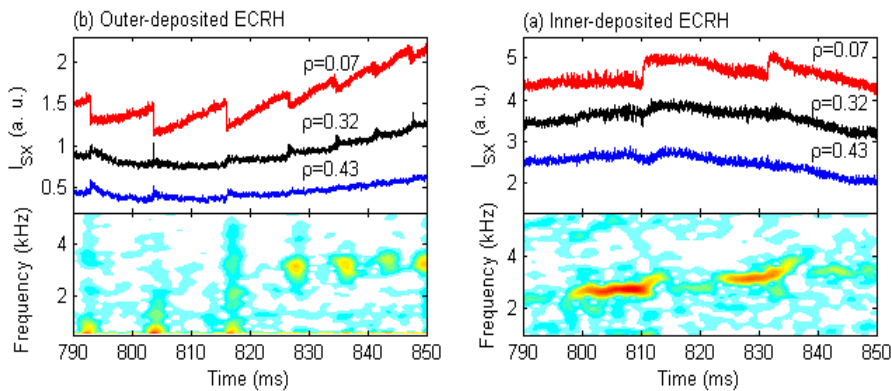


FIG. 8. Time revolutions of SXR signals (top) and frequency spectrum at central SXR chord in (a) outer- and (b) inner-deposited ECRH.

related to the impurity transport.

In order to study the effect of inner-deposited ECRH with the long-lasting  $m/n=1/1$  mode on the impurity transport, aluminum is injected as the trace impurity. The impurity diffusion coefficient and the convection velocity are analyzed from the temporal behavior of SXR intensity signals after LBO using 1-D impurity transport code STRAHL. The result shows that the outward convective velocity is further increased during the inner-deposited ECRH, while the inward convective velocity is usually seen in the ohmic discharge. The simulated Al density profile also exhibits a slight hollow or flat profile during the inner-deposited ECRH. The present result strongly suggests that the deposition control of ECRH plays an important role on the impurity density profile flattening and the impurity accumulation mitigation.

### Acknowledgements

This work was partly supported by the National Natural Science Foundation of China (grant no. 11375057 and no. 11175061), Chinese National Magnetic Confinement Fusion Science Program (no. 2014GB108003), and the JSPS-NRF-NSFC A3 Foresight Program in the field of Plasma Physics (NSFC: No.11261140328, NRF: No.2012K2A2A6000443).

### References

- [1] Neu, R., et al., Plasma Phys. Control. Fusion **44** (2002) 811.
- [2] Hong, J., et al., Nucl. Fusion **55** (2015) 063016.
- [3] Cui, Z.Y., et al., Nucl. Fusion **53** (2013) 093001.
- [4] Argioni, C., et al., Phys. Rev. Lett. **96** (2006) 095003.
- [5] Dux, R., et al., Nucl. Fusion **39** (1999) 1509.
- [6] Sertoli, M., et al., Plasma Phys. Control. Fusion **57** (2015) 075004.
- [7] Weisen, H., et al., Nucl. Fusion **41** (2001) 1227.
- [8] Dux, R., 2006, Technical Report No 10/30, IPP-Garching, Germany.
- [9] Summers, H.P., 2000, The ADAS User Manual version 2.2 <http://adas.phys.strath.ac.uk>
- [10] Sertoli, M., et al., Plasma Phys. Control. Fusion **53** (2011) 035024.
- [11] Cui, X., et al., Chin. Phys. B **22** (2013) 125201.